J. Fluid Mech. (2013), *vol.* 731, *pp.* 142–161. © Cambridge University Press 2013
doi:10.1017/jfm.2013.373

Rise in optimized capillary channels

B. Figliuzzi† and C. R. Buie

Department of mechanical Engineering, Massachusetts Institute of Technology, Cambridge, 77 Massachusetts Avenue, MA 02139, USA

(Received 22 March 2013; revised 16 June 2013; accepted 15 July 2013; first published online 14 August 2013)

Many technological applications rely on the phenomenon of wicking flow induced by capillarity. However, despite a continuing interest in the subject, the influence of the capillary geometry on the wicking dynamics remains underexploited. In numerous applications, the ability to promote wicking in a capillary is a key issue. In this article, a model describing the capillary rise of a liquid in a capillary of varying circular cross-section is presented. The wicking dynamics is described by an ordinary differential equation with a term dependent upon the shape of the capillary channel. Using optimal control theory, we were able to design optimized capillaries which promote faster wicking than uniform cylinders. Numerical simulations show that the height of the rising liquid was up to 50 % greater with the optimized shapes than with a uniform cylinder of optimal radius. Experiments on specially designed capillaries with silicone oil show a good agreement with the theory. The methods presented can be useful in the design and optimization of systems employing capillary-driven transport including micro-heat pipes or oil extracting devices.

Key words: capillary flows, control theory, flow control

1. Introduction

When a capillary of sufficiently small diameter is dipped in a bath of a wetting liquid, the liquid rises in the capillary under the action of surface tension until it reaches a height where surface tension forces are balanced by gravitational forces. This effect has been known since at least the 18th century through the experimental works of Newton, Hauksbee, Hooke and Jurin. An historical background can be found in the classical textbook of De Gennes, Brochard-Wyart & Quéré (2003). Wetting properties of liquids have been exploited in many engineered systems and natural processes, with applications in oil recovery, inkjet printing and in various other fields. The wicking dynamics in a capillary was first modelled a century ago, when pioneering works of Bell & Cameron (1906), Lucas (1918) and Washburn (1921) established that for a capillary of constant cross-section, the position of the meniscus is proportional to $\sqrt{t}$, where t is time, a result usually referred to as Washburn's law. In their model, Washburn and Lucas demonstrate that the wicking dynamics is described by the ordinary differential equation

$$\dot{h} = \frac{2\sigma \cos\theta R - \rho g h R^2}{8\mu h}, \tag{1.1}$$

† Email address for correspondence: crb@mit.edu

https://doi.org/10.1017/jfm.2013.373 Published online by Cambridge University Press

where R denotes the capillary radius, h the rise height, σ air–liquid surface tension, θ equilibrium contact angle (De Gennes 1985), g gravitational acceleration, and ρ and μ the liquid density and dynamic viscosity respectively. Since its formulation, the Washburn–Lucas equation has constituted the basis of nearly all models aimed at describing capillary rise in a circular capillary and has been used to account for various experimental results (Stange, Dreyer & Rath 2003). However, the Washburn–Lucas model is only valid in a specific context. As evidenced by Bosanquet (1923), it is inadequate at very short times, where it leads to an unphysical infinite imbibition velocity:

$$\dot{h} \to \infty \quad \text{when } h \to 0. \tag{1.2}$$

Subsequently, the Washburn and Lucas model has been improved during the last century. Szekely, Neumann & Chuang (1971) presented a rigorous formulation of the Washburn–Lucas equation which properly composes the energy balance for the entry flow and is consequently valid at short times. Other approaches have been developed to remove the singularity of the velocity at $t = 0$. Zhmud, Tiberg & Hallstensson (2000) proposed introducing an effective initial height λ at the beginning of the capillary rise. Mass conservation can be used to estimate the value of λ. The amount of liquid displaced at the beginning of the capillary rise is indeed not limited to the infinitesimal amount which rises in the capillary channel, but also includes the liquid of the bath which is put in motion. In other work related to capillary rise, Fries & Dreyer (2008*a*) derived an analytical solution for the Washburn–Lucas equation. They also explored the case of low-viscosity fluids, where the wicking dynamics is dominated by inertial forces (Fries & Dreyer 2008*b*). For such fluids, Queré and co-workers demonstrated the occurrence of oscillations around the equilibrium position of the meniscus (Quéré 1997; Quéré, Raphael & Ollitrault 1999; Lorenceau *et al.* 2002). More recently, the case of non-Newtonian power-law liquids was investigated by Digilov (2008).

The influence of the capillary channel geometry on the wicking dynamics has been investigated in numerous studies. Staples & Shaffer (2002) considered the wicking of a liquid in a capillary channel of circular cross-section whose diameter varies with a sinusoidal law to improve the understanding of capillary flow in porous media. Erickson, Li & Park (2002) conducted numerical simulations based on the resolution of the Navier–Stokes equation to model capillary-driven flows in diverging–converging and converging–diverging cross-sectional capillaries, showing that these configurations exhibit significantly slower wetting behaviour than straight capillaries. More recently, Reyssat *et al.* (2008) studied imbibition in capillary channels with axial variations and demonstrated that the imbibition dynamics is closely related to the details of the geometry of the capillary channel at long times. Various shapes have also been considered, including stepped capillary tubes (Erickson *et al.* 2002; Polzin & Choueiri 2003; Young 2004), V-shaped open grooves (Romero & Yost 1996; Rye, Mann & Yost 1996; Weislogel & Litcher 1998; Dussaud, Adler & Lips 2003; Warren 2004), assemblies of parallel cylinders (Princen 1969) or corner flows (Higuera, Medina & Linan 2008; Ponomarenko, Quéré & Clanet 2011). To our knowledge, none of these studies were aimed at optimizing geometry for fast transport.

As noted in the study conducted by Reyssat *et al.* (2008), capillary geometry can have a significant influence on the wicking dynamics. The design of an optimized shape promoting fast wicking is then of interest regarding the development of passive devices aimed at transporting fluids through capillary effects. Such devices are encountered in many applications. Capillary-driven flows are exploited to transport

https://doi.org/10.1017/jfm.2013.373 Published online by Cambridge University Press

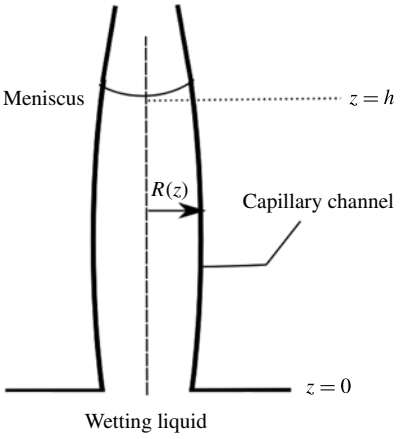


FIGURE 1. Capillary channel with varying circular cross-section.

fluids in the absence of gravitational effects. Processes including circulation and separation of large quantities of water in spacecraft life support systems were addressed in Weislogel, Thomas & Graf (2009). Engineered microfluidic devices such as capillary-driven heat pipes are another important application of capillary rise phenomena (Suman & Kumar 2005; Sobhan, Rag & Peterson 2007; Zhang, Watson & Wong 2007). For these devices, coolant circulation is ensured by capillary effects. Finally, in the oil industry, developing optimized capillaries could be critical for improving the performance of absorbent structures.

In this work, we present a theoretical method which allows the design of capillary channels whose shapes promote fast wicking. In § 2, a mathematical model is developed which extends the Washburn–Lucas equation to the case of capillary channels with varying circular cross-section. Numerical simulations based on this model are presented and compared to results found in the literature. Section 3 is devoted to the presentation of an optimization method based on control theory, facilitating the design of shapes promoting faster transport than uniform cylindrical capillaries. The results of the optimization method are discussed in § 4 and conclusions are drawn in § 5.

2. Capillary rise in a capillary channel of varying circular cross-section

2.1. *Mathematical model*

In this section we present a model describing the capillary rise of a liquid in a tube of varying circular cross-section. The case of horizontal cones has already been treated in Reyssat *et al.* (2008). The cross-section of the capillary channel remains circular, but the radius of each cross-section is allowed to vary with the capillary height, as shown on figure 1. The incompressible flow is treated as one-dimensional in the vertical or z-direction, where we denote the radius $R(z)$ at height z. The classical Hagen–Poiseuille description is used to describe the wicking dynamics; $h(t)$ is the height reached by the liquid at time t in the capillary. By convention, $z = 0$ indicates the location of the opening. The Hagen–Poiseuille description remains valid at low Reynolds numbers and for shapes where $|\mathrm{d}R/\mathrm{d}z| \ll 1$. In this description, the velocity

https://doi.org/10.1017/jfm.2013.373 Published online by Cambridge University Press

profile is given by

$$v(r) = \frac{1}{4\mu}\left(\frac{\partial p}{\partial z} + \rho g\right)(r^2 - R^2), \tag{2.1}$$

where r denotes the position coordinate in cylindric coordinates, μ the viscosity of the fluid, and p the pressure. At the boundary $r = R$, the velocity vanishes, as imposed by the no-slip boundary condition. We can easily deduce from (2.1) the volumetric flow rate as a function of the pressure gradient,

$$\dot{V} = -\frac{R^4\pi}{8\mu}\left(\frac{\partial p}{\partial z} + \rho g\right). \tag{2.2}$$

We further assume that the fluid wets the capillary. At the meniscus which forms at position $h(z)$, the liquid pressure is $p = p_0 - \sigma\kappa$, where σ denotes the surface tension of the film and κ the radius of curvature. In our case, if we take into account the slope of the capillary channel and the contact angle of the liquid on the capillary channel, θ, we find

$$P_{z=h} = -\frac{2\sigma\cos\left(\theta + \arctan\dfrac{\mathrm{d}R}{\mathrm{d}h}(h)\right)}{R(h)}. \tag{2.3}$$

We can next integrate expression (2.2) between $z = 0$, where the pressure is $P_{z=0} = 0$, and $z = h$ to find:

$$\frac{2\sigma\cos\left(\theta + \arctan\dfrac{\mathrm{d}R}{\mathrm{d}h}(h)\right)}{R(h)} - \rho g h = -8\mu\frac{\dot{V}}{\pi}\int_0^h \frac{\mathrm{d}z}{R(z)^4}. \tag{2.4}$$

The driving force ΔP corresponds to the difference between the capillary suction pressure developing at the meniscus and the hydrostatic pressure at the base of the fluid column. Using mass conservation equation

$$\dot{V} = \pi R(h)^2\dot{h}, \tag{2.5}$$

we finally obtain a first-order differential equation describing the rise of the liquid in the capillary:

$$\frac{2\sigma\cos\left(\theta + \arctan\dfrac{\mathrm{d}R}{\mathrm{d}h}(h)\right)}{R(h)} - \rho g h = -8\mu R(h)^2\dot{h}\int_0^h \frac{\mathrm{d}z}{R(z)^4}. \tag{2.6}$$

We can write this equation in explicit form, to yield

$$\dot{h} = \frac{2\sigma\cos\left(\theta + \arctan\dfrac{\mathrm{d}R}{\mathrm{d}h}(h)\right) - \rho g h R(h)}{8\mu R(h)^3\displaystyle\int_0^h \frac{\mathrm{d}z}{R(z)^4}}. \tag{2.7}$$

If we neglect the curvature of the capillary channel, we obtain the simplified equation

$$\dot{h} = \frac{2\sigma\cos\theta - \rho g h R(h)}{8\mu R(h)^3\displaystyle\int_0^h \frac{\mathrm{d}z}{R(z)^4}}. \tag{2.8}$$

https://doi.org/10.1017/jfm.2013.373 Published online by Cambridge University Press

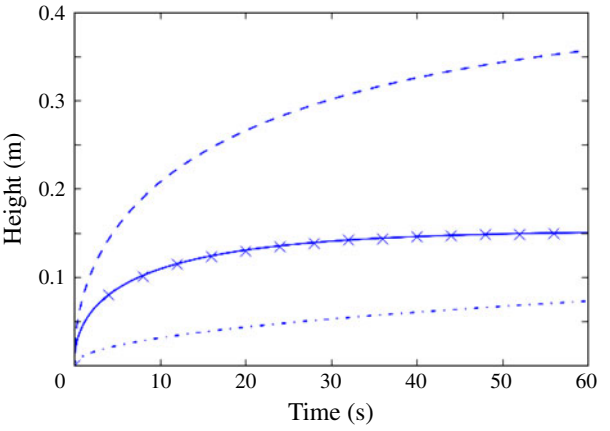


FIGURE 2. (Colour online) Influence of the physical parameters of the liquid on the dynamics of the capillary rise. The following values of parameters have been used: $\sigma = 7.5 \times 10^{-2}$ N m^{-1}, $\rho = 1000$ kg m^{-3}, $\mu = 1.5 \times 10^{-3}$ Pa s. For the highest curve, the surface tension is changed to $\sigma = 0.2$ N m^{-1}. For the lowest curve, the viscosity is changed to $\mu = 0.1$ Pa s. The continuous line shows results of the numerical simulation for the selected parameters, compared to the analytical expression found by Fries & Dreyer (2008*a*) (crosses).

This equation is identical to the one obtained by Staples & Shaffer (2002) and Reyssat *et al.* (2008). Note that Reyssat *et al.* (2008) only considered the case of horizontal capillary channels. For a uniform cylinder of constant radius R, we recover the Washburn–Lucas equation:

$$\dot{h} = f(h, R) = \frac{\sigma \cos\theta R}{4\mu h} - \frac{\rho g R^2}{8\mu}. \tag{2.9}$$

2.2. *Numerical analysis*

Solution of (2.7) can be carried out numerically through a second-order Runge–Kutta method with adaptive step size. Since the dynamics of the capillary rise slows down throughout the process, the use of an adaptive step size is an efficient way to reach a specified accuracy without unnecessary small integration steps. Figure 2 shows the influence of different fluid properties on the dynamics of capillary rise for a cylinder of radius $R = 100$ μm. The results of the numerical simulation are compared to the analytical expression found by Fries & Dreyer (2008*a*).

Investigations on the influence of capillary geometry on the wicking dynamics have been performed in numerous studies. Reyssat *et al.* (2008) investigated the imbibition dynamics in horizontal porous geometries with axial variation. Capillary channels with shapes given by

$$R(z) = R_0 + \alpha z^n \tag{2.10}$$

were considered, where $R(z)$ denotes the radius of the circular cross-section of the capillary channel at position z, and α is a positive parameter. An analytical model is developed, which directly relates the exponent n to the imbibition dynamics. For instance, for $n = 2$, α has the dimension of the inverse of a length and it is found that

$$87H^2 + 58H^4 + 15H^6 - 24\ln(1 + H^2) + (105 + 105H^2 + 63H^4 + 15H^6)H \arctan(H) = 42T, \tag{2.11}$$

https://doi.org/10.1017/jfm.2013.373 Published online by Cambridge University Press

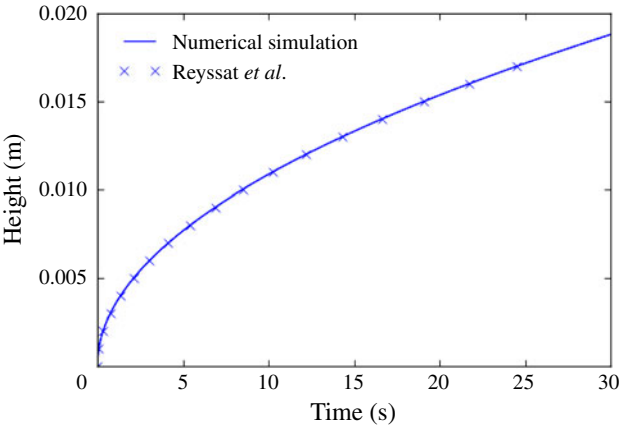


FIGURE 3. (Colour online) Comparison between the results of the numerical simulation and the analytic solution of Reyssat *et al.* (2008). The following values of parameters were used: $\sigma = 0.2$ N m^{-1}, $\mu = 0.1$ Pa s, $\theta = 0°$, $\alpha = 0.003$ m^{-1}, $R_0 = 1.09$ mm.

where the dimensionless parameters H and T are given by

$$\left.\begin{aligned} H &= h\sqrt{\frac{\alpha}{R(0)}}, \\ T &= \frac{2\sigma\alpha t}{\mu}. \end{aligned}\right\} \tag{2.12}$$

Figure 3 compares the results obtained with our numerical code to the analytical solution of Reyssat *et al.* (2008) for a parabolically shaped channel. An excellent agreement is found.

Erickson *et al.* (2002) performed their study of capillary rise with a completely different approach; instead of using the Washburn–Lucas equation, they numerically solve the complete Navier–Stokes equations to describe imbibition dynamics. In their article, diverging–converging and converging–diverging capillaries are considered, as shown in figure 4. Figure 5 compares their results to our numerical code. Good agreement is found, demonstrating the validity of the Poiseuille–Hagen approach for the study of capillary rise for cylindrical capillaries with slowly varying cross-sections.

3. Shape optimization

Numerous papers on the topic of capillary rise investigate the influence of the capillary shape on wicking dynamics. However, to our knowledge, none of these studies were aimed at designing optimal capillary geometries. This section presents a method to design shapes which promote fast wicking. First we investigate the determination of the optimal radius for a cylindrical capillary channel. Despite its simplicity, this question is of interest to better understand the underlying physics of the problem. The optimization problem for general shapes, described by any positive function $z \to R(z)$, is extremely complicated to solve due to the algebraic complexity of the model equations and the size of the set of all possible solutions. However, we can restrict the set of solutions and consider capillary channels whose shapes are described by an equation involving n scalar parameters. The problem then becomes the determination of the n optimized parameters that improve the wicking properties of the

https://doi.org/10.1017/jfm.2013.373 Published online by Cambridge University Press

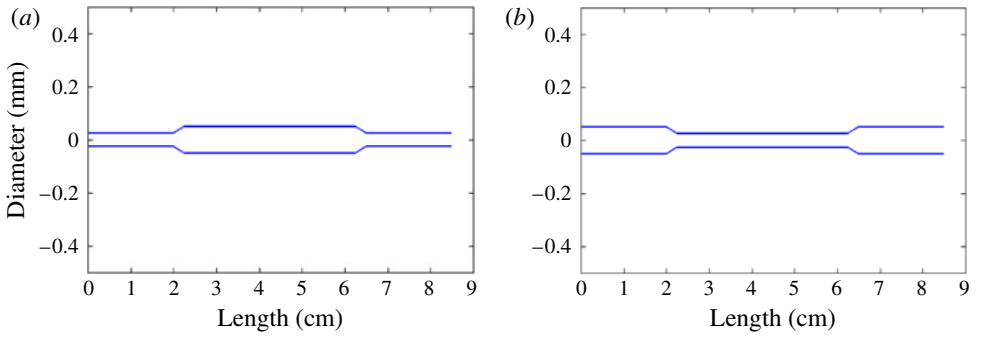


FIGURE 4. (Colour online) (*a*) Diverging–converging and (*b*) converging–diverging channels considered in Erickson *et al.* (2002).

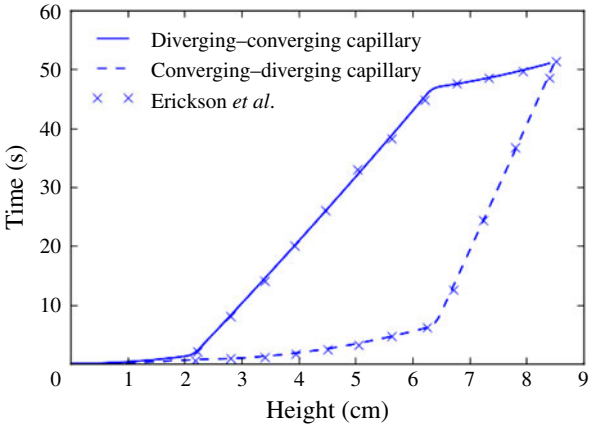


FIGURE 5. (Colour online) Comparison between the results of the numerical simulation and the solution of Erickson *et al.* (2002). The following values of parameters were used: $\sigma = 0.03$ N m^{-1}, $\mu = 0.001$ Pa s, $\theta = 30°$.

capillary. By proceeding in this fashion, we are able to considerably reduce the set of all possible shapes, while maintaining enough degrees of freedom to obtain significant improvement of the design of the capillary channels.

3.1. *The optimal cylinder*

In the case of a uniform cylinder, the wicking dynamics is described by the first-order differential equation (2.9), whose second term depends on the radius R of the cylinder. If we specify an arbitrary amount of time T, it is possible to determine an optimal radius R which maximizes the height reached by the liquid rising in the cylinder at time T. The wicking dynamics is the result of an interplay between three physical effects. First, surface tension, which is assumed constant during the entire capillary rise, results in a capillary pressure P_σ which pulls the liquid into the capillary. Next, the hydrostatic pressure and the viscous effects, which increase with the height of the liquid column, oppose the rise of the fluid. Unlike the capillary and the hydrostatics pressure, which both directly depend on the cylinder radius, viscous effects are proportional to the meniscus velocity and are therefore influenced

https://doi.org/10.1017/jfm.2013.373 Published online by Cambridge University Press

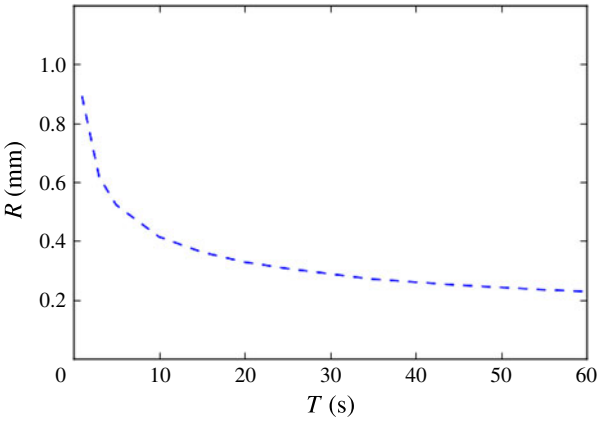


FIGURE 6. (Colour online) Optimal radius R for different specified time T. The following values of parameters have been used: $\sigma = 0.021\ \mathrm{N\ m^{-1}}$, $\theta = 0°$, $\rho = 980\ \mathrm{kg\ m^{-3}}$, $g = 9.81\ \mathrm{N\ kg^{-1}}$.

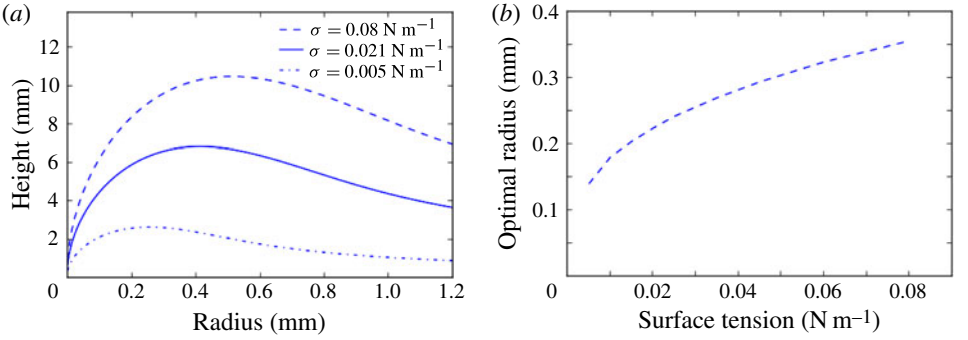


FIGURE 7. (Colour online) (*a*) Height reached by a liquid rising in a cylinder after $t = 10$ s as a function of the radius R of the cylinder for different values of the surface tension. (*b*) Optimal radius as a function of surface tension. The following values of parameters have been used: $\mu = 0.5$ Pa s, $\theta = 0°$, $\rho = 980\ \mathrm{kg\ m^{-3}}$, $g = 9.81\ \mathrm{N\ kg^{-1}}$.

by the dynamics of the capillary rise. The optimal radius consequently varies with the specified time T, as shown in figure 6. We note that the optimal radius decreases when specified time T is increased. This is partly due to hydrostatic pressure effects. Their influence is negligible at the beginning of capillary rise when h remains small, which explains why at short times larger radii are favoured. Figure 7(*a*) shows the height reached by a liquid rising in a cylinder after $t = 10$ s as a function of the cylinder radius, for different values of surface tension. As expected, optimal radius increases with surface tension. Similarly, figure 8(*a*) shows that the height reached by a liquid rising in a cylinder after $t = 10$ s is a function of the cylinder radius for different values of viscosity. We note that an increase in viscosity results in a larger optimal radius (figures 7*b* and 8*b*).

https://doi.org/10.1017/jfm.2013.373 Published online by Cambridge University Press

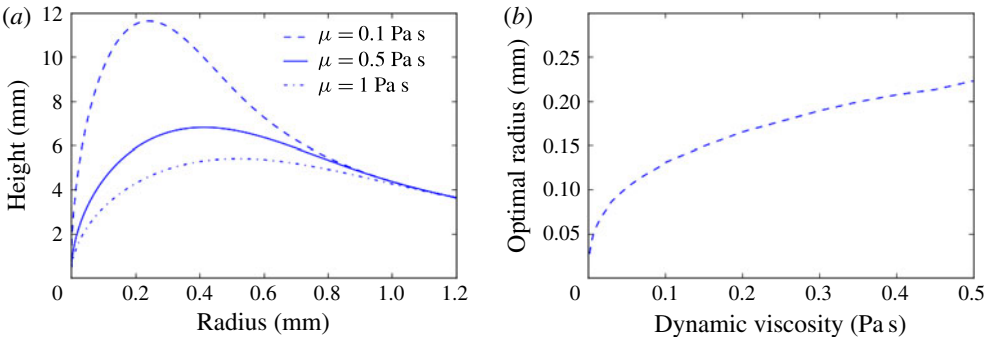


FIGURE 8. (Colour online) (*a*) Height reached by a liquid rising in a cylinder after $t = 10$ s as a function of the radius R of the cylinder for different values of the dynamic viscosity. (*b*) Optimal radius as a function of dynamic viscosity. The following values of parameters have been used: $\sigma = 0.021$ N m^{-1}, $\theta = 0°$, $\rho = 980$ kg m^{-3}, $g = 9.81$ N kg^{-1}.

3.2. *Parametric approach*

Though analytical solutions of the optimization problem seem out of reach, numerical approaches can nevertheless be considered. Here, we rely on a method based on a prior shape parametrization. The optimization problem then becomes the determination of the optimal parameters defining the shape. If we adopt the point of view of optimal control (Lewis, Vrabie & Syrmos 2012), these parameters can be seen as control parameters of the dynamical system described by (2.7).

3.2.1. *Theory*

Let $\Delta h > 0$ be an arbitrary positive real number. In this section, we will restrict considerations to the set $S_{\Delta h}$ of all shapes of the form $R = R(z, r_0, \dots r_N)$ which depend on $N + 1$ scalar parameters, and whose equation is given by

$$R(z, r_0, \dots, r_N) = \sum_{k=0}^{N-1} \left[\frac{r_{k+1} - r_k}{\Delta h}(z - k\Delta h) + r_k \right] \mathbf{1}_{[k\Delta h,(k+1)\Delta h]}(z), \tag{3.1}$$

where $\mathbf{1}$ denotes the indicative function of the interval $[k\Delta h, (k+1)\Delta h]$. The parameter r_k defines the value of the radius of the capillary channel at height $k\Delta h$. The radius values at the intermediate heights between $k\Delta h$ and $(k+1)\Delta h$ are deduced from r_k and r_{k+1} by linear interpolation. The set $S_{\Delta h}$ contains all possible discretized shapes with a discretization step Δh. A last requirement on the set of admissible shapes is dictated by a practical consideration: our aim is to design shapes whose radius remains large enough so that practical application can be considered for the capillary channel. An easy way to ensure this is to fix the outlet radius of the capillary channel to a value r, r being a positive real number. In mathematical terms, we restrict the set of solutions to the subset

$$S_{\Delta h,r} = \{R \in S_{\Delta h}, R(N\Delta h) = r\}. \tag{3.2}$$

In addition, the capillary radius must remain below the capillary length l_c, defined by

$$l_c = \sqrt{\frac{\sigma \cos\theta}{\rho g}}, \tag{3.3}$$

https://doi.org/10.1017/jfm.2013.373 Published online by Cambridge University Press

which compares the relative effects of surface tension and gravity. Then, $\forall i, 0 \leqslant i \leqslant N-1$, $r_i \in [0, l_c]$.

At this point, we consider the following problem: having arbitrarily fixed a given amount of time T, we try to determine the shape $R(z)$ in $S_{r,\Delta h}$, or more precisely the parameters $r_0, \ldots, r_{N-1}$, which maximizes the height $h(T)$ reached by the liquid at time T in the capillary channel. In mathematical terms, we try to minimize the cost

$$J(h) = -h(T), \tag{3.4}$$

under the constraint defined by the Washburn–Lucas equation (2.7), which can be recast as

$$\left.\begin{aligned} \dot{h} &= \frac{2\sigma\cos\left(\theta + \arctan\dfrac{\mathrm{d}R}{\mathrm{d}h}(h)\right) - \rho g h R(h)}{8\mu R(h)^3 \displaystyle\int_0^h \frac{\mathrm{d}z}{R(z)^4}} \\ &= f(h, r(h, r_0, \ldots r_N)) = f(h, r_0, \ldots, r_N), \\ h(0) &= \lambda. \end{aligned}\right\} \tag{3.5}$$

The cost functional (3.4) enables us to properly define the optimization problem. By simply modifying the definition of this functional, it is possible to solve similar optimization problems related to capillary rise. For instance, to obtain the shape that maximizes the extracted volume of fluid in a given time, the cost functional has to be modified to yield

$$J(h) = \int_0^{h(T)} \pi R(z)^2 \,\mathrm{d}z. \tag{3.6}$$

In (3.5), the radius varies with height according to relation (3.1). The parameters $r_0, \ldots, r_N$ belong to the compact set $[0, l_c]$; λ is the effective initial height introduced by Zhmud *et al.* (2000) to remove the singularity of the velocity at $t = 0$; f is Lipschitz continuous on its definition domain.

PROPOSITION 1. *We consider the function $\tilde{J}$ defined on $M \times C^1([0,T]) \times [0, l_c]^{N+1}$ by*

$$\tilde{J}(p, h, r_0, \ldots, r_N) = -h(T) + \int_0^T p(t)(f(h, r(h)) - \dot{h})\,\mathrm{d}t, \tag{3.7}$$

where M denotes the space of differentiable functions and $C^1([0,T])$ the space of continuously differentiable functions $[0,T] \to \mathbb{R}_+$. If $(p, h, r_0, \ldots, r_N)$ is a stationary point of $\tilde{J}$, then $(h, r_0, \ldots, r_N)$ is a stationary point of J which satisfies constraint (3.5).

Proof. The proof of proposition 1 is developed in appendix A. □

According to proposition 1, the problem that we consider is equivalent to the determination of the stationary points of the function $\tilde{J}$ defined by (3.7). Given fixed parameters $r_0, \ldots, r_N$, for the constraint to be verified, the function $t \to h(t)$ has to be defined by the Cauchy problem

$$\left.\begin{aligned} \dot{h} &= f(h, r_0, \ldots, r_N), \\ h(0) &= \lambda. \end{aligned}\right\} \tag{3.8}$$

https://doi.org/10.1017/jfm.2013.373 Published online by Cambridge University Press

This problem has a unique solution, which means that the function $t \to h(t)$ is entirely determined by the set of parameters $\{r_0, \ldots, r_N\}$. Similarly, the function p can be shown to be defined uniquely by the Cauchy problem

$$\left.\begin{aligned} \dot{p}(t) &= -p(t)\frac{\partial f}{\partial h}(h, r_0, \ldots, r_N), \\ p(T) &= -1. \end{aligned}\right\} \tag{3.9}$$

The value of $\tilde{J}$ then only depends on the parameters $r_0, r_1, \ldots, r_N$:

$$\tilde{J}(p, h, r_0, \ldots, r_N) = \tilde{J}(r_0, \ldots, r_N). \tag{3.10}$$

Moreover, $\forall i \in [0, N]$, the value of the gradient of $\tilde{J}$ with respect to r_i, given by

$$\frac{\partial \tilde{J}}{\partial r_i}(p, h, r_0, \ldots, r_N) = \int_0^{+\infty} p(t)\frac{\partial f}{\partial r_i}(h, r_0, \ldots, r_N)\,\mathrm{d}t, \tag{3.11}$$

only depends on the set of parameters $\{r_0, r_1, \ldots, r_N\}$. The problem we are left with is then the determination of the stationary points of the functional $\tilde{J}$ on the set $[0, l_c]^{N+1}$. This set is compact, which ensures the existence and the uniqueness of a global minimum. However, as the function $\tilde{J}$ is not convex, a stationary point does not necessarily constitute a global minimum. Starting from an arbitrary shape, like for instance the optimal cylinder, we can still reasonably hope to significantly improve the design of the shape. As we are able to calculate the function $\tilde{J}$ and its gradient, a steepest-descent method can be used to find a local minimum of $\tilde{J}$, as described in appendix B.

4. Results and discussion

Figures 9 and 10 show the optimal shape found for water and silicone oil respectively using the numerical algorithm described in the previous section. Both shapes have been designed to maximize the height reached by the liquid at time $T = 60$ s. The radius of the outlet of both capillary channels is arbitrarily fixed and is equal to $R_{out} = 42$ μm for the water and $R_{out} = 336$ μm for the silicone oil. These values correspond to the optimal cylinder radius for both fluids regarding wicking performance, determined numerically. The dynamics of the capillary rise in the optimized capillary channel is compared to the dynamics of the capillary rise in a cylinder of radius R_{out} and in the optimal cone of outlet radius R_{out}. If we consider a conic shape of opening angle α, the capillary rise equation becomes

$$\frac{\mathrm{d}h}{\mathrm{d}t} = \frac{2R_0\sigma\cos(\theta+\alpha) - \rho g h R_0 - \rho g \tan(\alpha) h^2}{8\mu h\left(1 + \dfrac{\tan(\alpha)h}{R_0} + \dfrac{\tan^2(\alpha)h^2}{R_0^2}\right)}. \tag{4.1}$$

This equation is much simpler than the general equation for capillaries with varying circular cross-section, but the optimization of the underlying dynamical system remains very difficult to handle analytically. We consequently relied on the general numerical method developed in this paper to determine the optimal conic shapes presented in figures 9 and 10.

The two optimal non-cylindrical shapes present many similarities: they both exhibit a large radius at their bases in comparison with the radius of the outlet, and their radius is decreasing with the height of the capillary channel. The diverging section

https://doi.org/10.1017/jfm.2013.373 Published online by Cambridge University Press

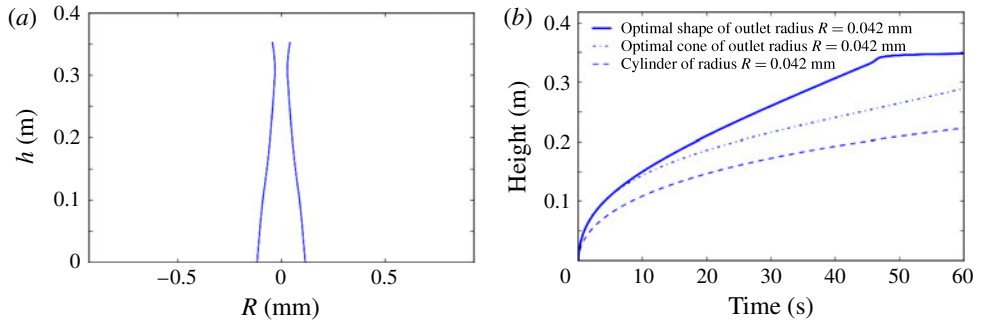


FIGURE 9. (Colour online) (*a*) Optimal shape found for the capillary channel in the case of water for $T = 60$ s. (*b*) The dynamics of the capillary rise is compared to the rise in the cylinder of optimal radius and in the optimal cone. The following values of parameters have been used: $\sigma = 0.0728$ N m^{-1}, $\theta = 0°$, $\rho = 1000$ kg m^{-3}, $g = 9.81$ N kg^{-1}, $\mu = 0.001$ Pa s, $\Delta h = 16$ mm.

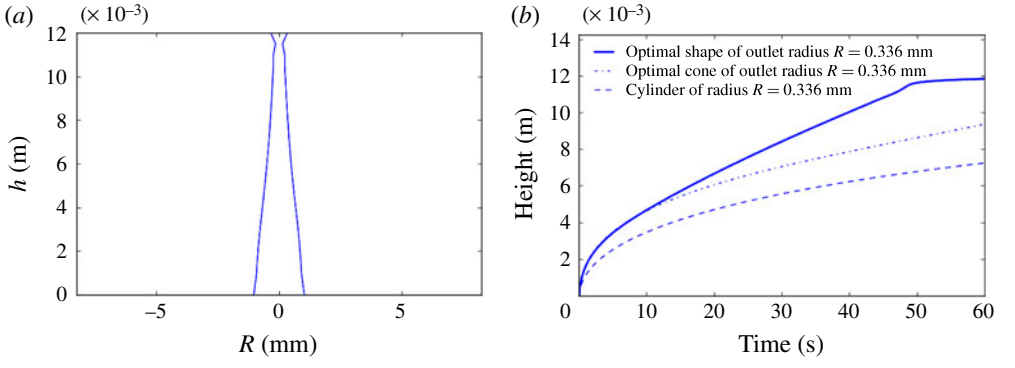


FIGURE 10. (Colour online) (*a*) Optimal shape found for the capillary channel in the case of silicone oil for $T = 60$ s. (*b*) The dynamics of the capillary rise is compared to the rise in the cylinder of optimal radius and in the optimal cone. The following parameter values have been used: $\sigma = 0.0295$ N m^{-1}, $\theta = 41°$, $\rho = 1095$ kg m^{-3}, $g = 9.81$ N kg^{-1}, $\mu = 2.45$ Pa s, $\Delta h = 0.5$ mm.

at the end of the capillary results from the arbitrary constraint imposed on the outlet radius of the capillary channel. We note that the wicking is significantly improved in both capillaries when compared with the case of the optimal cylinder. For water, the meniscus has reached a location 55.5 % higher in the optimized capillary than in the optimal cylinder at $T = 60$ s. For silicone oil, this value is around 60 %.

4.1. *Experiments*

The model developed in § 2 relies on the Poiseuille–Hagen equations to describe capillary rise. The Poiseuille–Hagen description is only valid for capillary channels with slowly varying radii, where $\mathrm{d}R/\mathrm{d}z \ll 1$. Experiments have been conducted to study the validity of the mathematical model developed in § 2 for a capillary channel whose shape is close to the optimal. The capillary channel used for the experiment was fabricated by pulling borosilicate glass capillaries with a P-2000 micropipette puller (Sutter Instrument). The precise manufacturing of capillary microchannels with

https://doi.org/10.1017/jfm.2013.373 Published online by Cambridge University Press

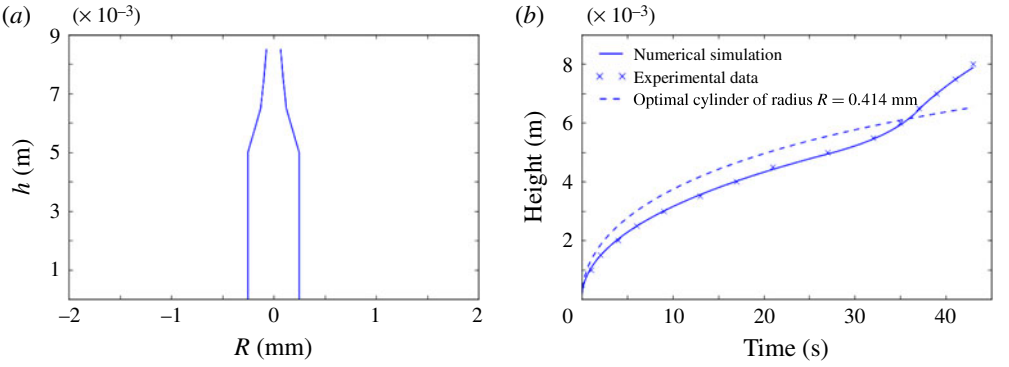


FIGURE 11. (Colour online) Comparison between the model and the experimental data. The model shows good agreement with the experimental data. We note that the shape of the capillary, shown in (*a*), has a significant influence on the rise dynamics. At $t = 30$ s, as shown in (*b*), the fluid reaches the location of the converging section of the capillary, which immediately influences the rise dynamics.

optimized shapes remains an open problem. However, using this technique, we were able to manufacture pulled capillaries close to the optimal design in the limiting case of highly viscous liquids. For these liquids, the high viscosity limits the length required for the capillary, which enables its manufacturing with the micropipette puller. The shape of the capillary, consisting of a cylinder followed by a converging section, is represented on figure 11(*a*). At the beginning of the experiment, the capillary channel is placed in contact with a reservoir of liquid. The rise of the liquid in the capillary is then monitored with a high-speed camera. The liquid used for the experiment is a silicone oil, whose physical parameters were measured to be $\sigma = 0.0295$ N m^{-1}, $\theta = 41°$, $\rho = 1095$ kg m^{-3}, $g = 9.81$ N kg^{-1}, $\mu = 2.45$ Pa s. The surface tension was obtained from Jurin's law by measuring the capillary height reached by the liquid in an uniform cylinder of specified radius. The dynamic contact angle θ was determined from the photographs of the meniscus taken with the camera. Finally, the viscosity was obtained by fitting the observed capillary rise with Washburn's law in the case of an uniform cylinder. Figure 11(*b*) compares the experimental measurements of the capillary rise to a numerical simulation of the mathematical model of § 2. The model fits the experimental data fairly well, which demonstrates that the mathematical model remains valid for the capillaries studied here. On the same figure, the dynamics of the capillary rise in the fabricated channel is compared to the capillary rise in the optimal cylinder for $T = 42$ s. We can note that at $T = 42$ s, the liquid has risen significantly higher (23 %) in the capillary used for the experiment than in the optimal cylinder.

4.2. *Dimensionless capillary rise equation*

To better understand the influence of the fluid geometry on the shape of the optimized capillaries, one can recast the Washburn–Lucas equation in terms of dimensionless variables. Here we consider the rise of a liquid in a vertical capillary channel of circular cross-section whose radius is given at each height by the positive function $z \to R(z)$. R_∞ denotes the radius of the cross-section located at the outlet, which is arbitrarily fixed for a given optimization problem. For a cylinder of radius R_∞, the

https://doi.org/10.1017/jfm.2013.373 Published online by Cambridge University Press

maximal height reached by the rising liquid is

$$h_\infty = \frac{2\sigma\cos\theta}{\rho g R_\infty}. \tag{4.2}$$

The height h of the meniscus and the radius R of the capillary channel can be rescaled using h_∞ and R_∞ respectively, which leads to the following dimensionless variables:

$$l = \frac{h}{h_\infty}, \quad r = \frac{R}{R_\infty}. \tag{4.3}$$

Similarly, we can rescale the time t using the arbitrary time T defined for the optimization problem:

$$\tau = \frac{t}{T}. \tag{4.4}$$

Substituting these variables in (2.7), we obtain

$$\frac{h_\infty}{T}\frac{\mathrm{d}l}{\mathrm{d}\tau} = \frac{2\sigma\cos\left[\theta + \arctan\left(\dfrac{R_\infty}{h_\infty}\dfrac{\mathrm{d}r}{\mathrm{d}z}\right)\right] - \rho g h_\infty R_\infty l r(h)}{8\mu\dfrac{h_\infty}{R_\infty} r(l)^3 \displaystyle\int_0^l \frac{\mathrm{d}z}{r(z)^4}}. \tag{4.5}$$

As the radius of the capillary channel is assumed to be slowly varying, we can assume that

$$\theta + \arctan\left(\frac{R_\infty}{h_\infty}\frac{\mathrm{d}r}{\mathrm{d}z}\right) \simeq \theta. \tag{4.6}$$

Equation (4.5) can then be recast to yield

$$K\frac{\mathrm{d}l}{\mathrm{d}\tau} = \frac{r(l) - l r(l)^2}{r(l)^4 \displaystyle\int_0^l \frac{\mathrm{d}z}{r(z)^4}}, \tag{4.7}$$

where K is a dimensionless number given by

$$K = \frac{16\mu\sigma\cos\theta}{T\rho^2 g^2 R_\infty^3} = \frac{\mu}{\rho g T R_\infty}\left(\frac{4l_c}{R_\infty}\right)^2. \tag{4.8}$$

In this relation, l_c denotes the capillary length of the liquid, defined by (3.3). One can identify a dimensionless viscous term in (4.7):

$$F_v(h) = K\dot{l} r(l)^4 \int_0^l \frac{\mathrm{d}z}{r(z)^4}. \tag{4.9}$$

This dimensionless viscous term is expressed as the product of the velocity of the meniscus $\dot{l}$ and of an effective dimensionless viscosity $\mu_{eff}(l)$ which depends upon the geometry of the capillary and is given by

$$\mu_{eff}(l) = K r(l)^4 \int_0^l \frac{\mathrm{d}z}{r(z)^4}. \tag{4.10}$$

https://doi.org/10.1017/jfm.2013.373 Published online by Cambridge University Press

In quasi-steady state, this dimensionless viscous term is exactly balanced by gravity and surface tension terms,

$$F_v(l) = F_d(l) = r(l) - lr(l)^2. \tag{4.11}$$

The capillary rise can be characterized in three phases. At short times, as l remains small, the integral in (4.10) is well approximated by

$$\int_0^l \frac{\mathrm{d}z}{r(z)^4} \simeq \frac{l}{r(l)^4}. \tag{4.12}$$

As discussed earlier, it is assumed that the radius of the capillary channel is slowly varying with height. Consequently, $\mu_{eff} \simeq l$. Similarly, the term $lr(l)^2$ can be neglected from (4.9) and (4.11), so that

$$Kl\dot{l} \simeq r(l). \tag{4.13}$$

It is clear from this relation that a large radius at the base of the capillary channel will favour wicking at the beginning of the capillary rise. The radius must however remain smaller than the capillary length.

For larger values of l, significant variations of the radius can occur between $z = 0$ and $z = l$, and approximation (4.12) is invalid. It can be shown that the effective viscosity μ_{eff} decreases with height l if the radius decreases with the height of the capillary,

$$\frac{\partial \mu_{eff}}{\partial z}(l) = 4\frac{\partial r}{\partial z}(l) r(l)^3 \int_0^l \frac{\mathrm{d}z}{r(z)^4} + 1. \tag{4.14}$$

Then, $\mu_{eff}(l)$ will decrease if and only if

$$\frac{\partial r}{\partial z}(l) < -\frac{1}{4r(l)^3 \displaystyle\int_0^l \frac{\mathrm{d}z}{r(z)^4}}. \tag{4.15}$$

This relation shows that increasing capillary channel radius with height reduces the meniscus velocity by increasing viscous effects. However, for sufficiently small values of l, surface tension remains the dominant effect on the driving force. Then, if the radius decreases with height, the dimensionless viscous term given by (4.11) also decreases. The resulting shape of the optimized capillary channel is an interplay between these two effects. Figure 12 compares the evolution of the viscous terms and of the effective viscosity μ_{eff} during the capillary rise of water for the optimal shape and the optimal cylinder. For the optimized shape, the viscous effects are greatly reduced in comparison with the cylinder shape. However, the decrease of the radius of the capillary with length limits the contribution of effective viscosity to the viscous effects, resulting in an increased rise velocity in comparison with the case of the optimal cylinder.

Finally, for large values of l, when gravity effects are the same order of magnitude as surface tension, a decrease in the radius with height increases the viscous forces. In the meantime, the contribution of the effective viscosity to the viscous effects is reduced. Consequently, the radius of the capillary channel rapidly decreases with height in the upper part of the capillary channel, as can be seen in figure 10.

https://doi.org/10.1017/jfm.2013.373 Published online by Cambridge University Press

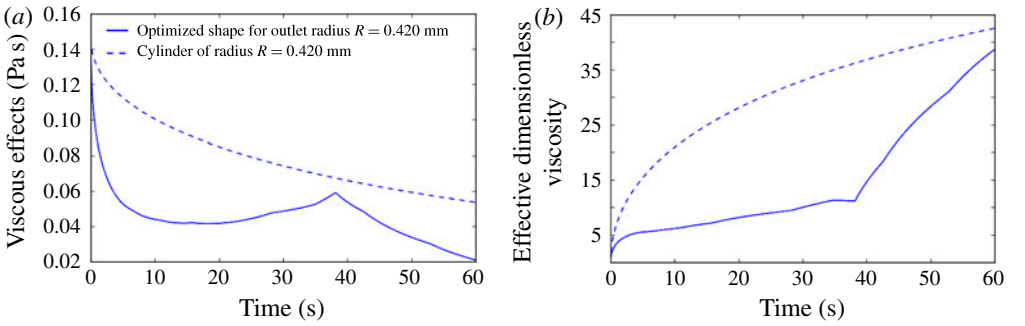


FIGURE 12. (Colour online) Evolution of (*a*) the viscous term F_v and (*b*) the effective viscosity μ_{eff} during the capillary rise in the optimized capillary channel and in the optimal cylinder in the case of water. The following values of parameters have been used: $\sigma = 0.021$ N m^{-1}, $\theta = 0°$, $\rho = 1000$ kg m^{-3}, $g = 9.81$ N kg^{-1}, $\mu = 0.001$ Pa s, $T = 60$ s.

5. Conclusion

The rise of a liquid in a capillary has received considerable attention in the scientific literature. However, the influence of capillary geometry has only been recently investigated. To our knowledge, Staples & Shaffer (2002) and Reyssat *et al.* (2008) established the first analytical models aimed at describing the rise of a liquid in a capillary with varying circular cross-section. In this article, an optimization method is presented to design optimized capillaries with circular cross-section for fast wicking. The liquid was shown to rise significantly higher in these optimized capillaries compared to optimal cylindrical geometry. Experiments performed with geometries close to the optimized capillary channels showed very good agreement with the mathematical model developed to predict capillary rise dynamics. The methods presented here can be useful in improving the design and optimization of systems employing capillary-driven transport, a method exploited in numerous applications including micro-heat pipes or oil extracting devices.

Several extensions of this study can be considered. The mathematical method used to optimize capillary shapes to promote fast wicking is quite general, and can easily be extended to solve other optimization problems. Examples include optimized geometries for maximizing flow rate or maximizing the amount of liquid dragged into the capillary. These problems could be of particular interest for the oil extraction industry.

Manufacturing capillaries with varying circular cross-section at low cost remains an open issue. To facilitate manufacturing, it could be of interest to extend the method developed to capillaries with non-circular cross-sections. Square capillaries are of particular interest as the manufacturing of such geometries can be performed quite easily. However, the rise of a liquid in a squared capillary differs significantly from the case of circular capillaries and this is an area of future research.

Acknowledgements

This work was sponsored by the Assistant Secretary for Defense for Research and Engineering (ASD(R&E)). We thank I. Hunter and J. Chang (Massachusetts Institute of Technology) for helpful discussions on the experimental part of this study. We are also grateful to F. Di Meglio (Ecole des Mines ParisTech) for his comments on the optimization method.

https://doi.org/10.1017/jfm.2013.373 Published online by Cambridge University Press

Appendix A. Proof of proposition 1

Let $(p, h, r_0, \ldots, r_N)$ in $M \times C^1([0, T]) \times [0, l_c]^{N+1}$ be a stationary point of functional $\tilde{J}$. Necessarily, for all admissible variation $t \to \delta h(t)$ of functional $t \to h(t)$, we have

$$\tilde{J}(p, h + \delta h, r_0, \ldots, r_N) - \tilde{J}(p, h, r_0, \ldots, r_N) = o(\delta h). \tag{A 1}$$

Using integration by parts and the initial condition $h(0) = \lambda$, where λ is a constant, we can show that

$$-\int_0^T \lambda(t)\delta\dot{h}(t)\,\mathrm{d}t = p(0)\lambda - p(T)\delta h(T) + \int_0^T \dot{p}(t)\delta h(t)\,\mathrm{d}t, \tag{A 2}$$

so that

$$\begin{aligned}\tilde{J}(p, h + \delta h, r_0, \ldots, r_N) - \tilde{J}(p, h, r_0, \ldots, r_N)\\ = -1 - p(T) + \int_0^T \left[p(t)\frac{\partial f}{\partial h}(h, r(h)) - \dot{p}(t)\right]\delta h(t)\,\mathrm{d}t + o(\delta h).\end{aligned} \tag{A 3}$$

Using the lemma of variations, we then obtain the two optimality conditions

$$\left.\begin{aligned} p(T) &= -1,\\ \dot{p}(t) &= -p(t)\frac{\partial f}{\partial h}(p, h, r_0, \ldots, r_N).\end{aligned}\right\} \tag{A 4}$$

We also have, for $0 \leqslant i \leqslant N$,

$$\frac{\partial \tilde{J}}{\partial r_i}(p, h, r_0, \ldots, r_N) = 0, \tag{A 5}$$

which leads to the condition

$$\int_0^T p(t)\frac{\partial f}{\partial r_i}(h, r_0, \ldots, r_N)\,\mathrm{d}t = 0. \tag{A 6}$$

Finally, we have, for all admissible variation of $t \to p(t)$,

$$\tilde{J}(p, h + \delta h, r_0, \ldots, r_N) - \tilde{J}(p, h, r_0, \ldots, r_N) = o(\delta h). \tag{A 7}$$

Using the lemma of variations, we obtain

$$\dot{h} = f(h, r_0, \ldots, r_N), \tag{A 8}$$

which gives us the constraint back. At this point, we consider an admissible infinitesimal variation $\mathrm{d}J$ of the functional J. We have, as conditions (A 4), (A 6) and (A 8) are satisfied,

$$\begin{aligned}\mathrm{d}J = -\delta h(T) = -\delta h(T) + \left[\sum_{i=0}^{N-1}\int_0^T p(t)\frac{\partial f}{\partial r_i}(h, r_0, \ldots, r_N)\,\mathrm{d}t\right]\delta r_i\\ + \int_0^T \left(p(t)\frac{\partial f}{\partial h}(h, \eta) + \dot{p}(t)\right)\delta h(t)\,\mathrm{d}t.\end{aligned} \tag{A 9}$$

https://doi.org/10.1017/jfm.2013.373 Published online by Cambridge University Press

Using integration by parts, we obtain

$$\begin{aligned} dJ &= -\delta h(T) + \left[\sum_{i=0}^{N-1} \int_0^T \lambda(t) \frac{\partial f}{\partial r_i}(h, r_0, \ldots, r_N)\, \mathrm{d}t\right] \delta r_i \\ &\quad + \int_0^T \lambda(t) \left(\frac{\partial f}{\partial h}(h, r_0, \ldots, r_N)\delta h - \dot{\delta h}\right) \mathrm{d}t + \lambda(T)\, \mathrm{d}h(T) \\ &= o(\delta h, \delta r_0, \ldots, \delta r_N). \end{aligned} \tag{A 10}$$

If $(p, h, r_0, \ldots, r_N)$ is a stationary point of $\tilde{J}$, then $(h, r_0, \ldots, r_N)$ is a stationary point of J which satisfies constraint (3.5).

Appendix B. Numerical resolution of the optimization problem

To solve the minimization problem considered in this article, a numerical steepest-descent method is used. We start with an arbitrary shape R_0 described by parameters $\{r_0^{(0)}, \ldots, r_N^{(0)}\}$. In practice, we will often start with a cylinder geometry where

$$r_0^{(0)} = r = \cdots = r_i^{(0)} = r = \cdots = r_N^{(0)} = r, \tag{B 1}$$

r being the outlet radius. Then, at each step n, we proceed as follows.

(a) The function $t \to h_n(t)$ is calculated by solving the Washburn–Lucas equation for the shape R_n, with initial condition $h_n(0) = 0$. The integration is performed using the Runge–Kutta scheme presented in § 2.

(b) The function $t \to p_n(t)$ is calculated by solving the reversed-time differential equation defining the Lagrangian multiplier, with initial condition $p(T) = -1$. A Runge–Kutta scheme of order two is used in this purpose.

(c) The gradient of $\tilde{J}$ is calculated:

$$\frac{\partial \tilde{J}}{\partial r_i}(r_0^{(n)}, \ldots, r_N^{(n)}) = \int_0^T \lambda(t) \frac{\partial f}{\partial r_i}(r_0^{(n)}, \ldots, r_N^{(n)})\, \mathrm{d}t. \tag{B 2}$$

The trapezoidal method is used to estimate the integrals that arise in this problem.

(d) The estimation of the optimized shape is then updated. $\forall i \in [0, N-1]$,

$$r_i^{(n+1)} = r_i^{(n)} - l^{(n)} \frac{\partial \tilde{J}}{\partial r_i}(r_0^{(n)}, \ldots, r_N^{(n)}). \tag{B 3}$$

This algorithm converges if the step $l^{(n)}$ is properly chosen at each step.

Definition 1. Let c_1 be a positive real number; $\forall n \in \mathbb{N}$, the inequality

$$\tilde{J}(\boldsymbol{r^{(n)}} + l^{(n)} \nabla \tilde{J}(\boldsymbol{r^{(n)}})) \leqslant \tilde{J}(\boldsymbol{r^{(n)}}) + c_1 l^{(n)} \|\nabla \tilde{J}(\boldsymbol{r^{(n)}})\|^2 \tag{B 4}$$

is called Armijo condition of parameter c_1 on the parameters $(l^{(n)}, \boldsymbol{r^{(n)}})_{n\in\mathbb{N}}$.

Definition 2. Let c_2 be a positive real number; $\forall n \in \mathbb{N}$, the inequality

$$\nabla \tilde{J}(\boldsymbol{r^{(n)}} + l^n \nabla \tilde{J})^{\mathrm{T}} \nabla \tilde{J}(\boldsymbol{r^{(n)}}) \geqslant c_2 \|\nabla \tilde{J}(\boldsymbol{r^{(n)}})\|^2 \tag{B 5}$$

is called the curvature condition of parameter c_2 on the parameters $(l^{(n)}, \boldsymbol{r^{(n)}})_{n\in\mathbb{N}}$. Conditions (B 4) and (B 5) with $0 < c_1 < c_2 < 1$ are referred to as Wolfe conditions.

https://doi.org/10.1017/jfm.2013.373 Published online by Cambridge University Press

PROPOSITION 2. *$\forall n \in \mathbb{N}$, there exists an interval $[l_1^{(n)}, l_2^{(n)}]$ so that $\forall l^{(n)} \in [l_1^{(n)}, l_2^{(n)}]$, the Wolfe conditions are satisfied.*

Proof. See for instance Bonnans *et al.* (2003). □

In the present case, the parameter $l^{(n)}$ is determined by using a line search strategy. The convergence of the algorithm is ensured by the following proposition.

PROPOSITION 3. *If the Wolfe conditions are satisfied at each step n, then the algorithm converges to a local stationary point of the functional $\tilde{J}$.*

Proof. See for instance Bonnans *et al.* (2003). □

REFERENCES

BELL, J. M. & CAMERON, F. K. 1906 The flow of liquids through capillary spaces. *J. Phys. Chem.* **10**, 657–674.

BONNANS, J., GILBERT, J., LEMARÉCHAL, C. & SAGASETIZBAL, C. 2003 *Numerical Optimization Theoretical and Practical Aspects*. Springer.

BOSANQUET, C. H. 1923 On the flow of liquids into capillary tubes. *Phil. Mag.* **45**, 525–531.

DE GENNES, P. G. 1985 Wetting: statics and dynamics. *Rev. Mod. Phys.* **57**, 827–863.

DE GENNES, P.-G., BROCHARD-WYART, F. & QUÉRÉ, D. 2003 *Capillarity and Wetting Phenomena: Drops, Bubbles, Pearls, Waves*. Springer.

DIGILOV, R. M. 2008 Capillary rise of a non-Newtonian power law liquid: impact of the fluid rheology and dynamic contact angle. *Langmuir* **24**, 13663–13667.

DUSSAUD, A. D., ADLER, P. M. & LIPS, A. 2003 Liquid transport in the networked microchannels of the skin surface. *Langmuir* **19**, 7341–7345.

ERICKSON, D., LI, D. & PARK, C. B. 2002 Numerical simulations of capillary-driven flows in nonuniform cross-sectional capillaries. *J. Colloid Interface Sci.* **250** (2), 422–430.

FRIES, N. & DREYER, M. 2008*a* An analytic solution of capillary rise restrained by gravity. *J. Colloid Interface Sci.* **320**, 259–263.

FRIES, N. & DREYER, M. 2008*b* The transition from inertial to viscous flow in capillary rise. *J. Colloid Interface Sci.* **327**, 125–128.

HIGUERA, F. J., MEDINA, A. & LINAN, A. 2008 Capillary rise of a liquid between two vertical plates making a small angle. *Phys. Fluids* **20**, 102102.

LEWIS, F. L., VRABIE, D. & SYRMOS, V. L. 2012 *Optimal Control*. Wiley.

LORENCEAU, E., QUÉRÉ, D., OLLITRAULT, J.-Y. & CLANET, C. 2002 Gravitational oscillations of a liquid column. *Phys. Fluids* **14**, 1985–1992.

LUCAS, V. R. 1918 Uber das Zeitgesetz des Kapillaren Aufstiegs von Flssigkeiten. *Kolloidn. Z.* **23**, 15–22.

POLZIN, K. A. & CHOUEIRI, E. Y. 2003 A similarity parameter for capillary flows. *J. Phys.* D **36** (24), 3156.

PONOMARENKO, A., QUÉRÉ, D. & CLANET, C. 2011 A universal law for capillary rise in corners. *J. Fluid Mech.* **666**, 146–154.

PRINCEN, H. M. 1969 Capillary phenomena in assemblies of parallel cylinders: I. Capillary rise between two cylinders. *J. Colloid Interface Sci.* **30** (1), 69–75.

QUÉRÉ, D. 1997 Inertial capillary. *Europhys. Lett.* **39**, 533–538.

QUÉRÉ, D., RAPHAEL, E. & OLLITRAULT, J.-Y. 1999 Rebounds in a capillary tube. *Langmuir* **15**, 3679–3682.

REYSSAT, M., COURBIN, L., REYSSAT, E. & STONE, H. A. 2008 Imbibition in geometries with axial variations. *J. Fluid Mech.* **615**, 335–344.

ROMERO, L. A. & YOST, F. G. 1996 Flow in an open channel capillary. *J. Fluid Mech.* **322**, 109–129.

RYE, R. R., MANN, J. A. & YOST, F. G. 1996 The flow of liquids in surface grooves. *Langmuir* **12**, 555–565.

https://doi.org/10.1017/jfm.2013.373 Published online by Cambridge University Press

SOBHAN, C. B., RAG, R. L. & PETERSON, G. P. 2007 A review and comparative study of the investigations on micro heat pipes. *Intl J. Energy Res.* **31** (6–7), 664–688.

STANGE, M., DREYER, M. E. & RATH, H. J. 2003 Capillary driven flow in circular cylindrical tubes. *Phys. Fluids* **15**, 2587–2601.

STAPLES, T. L. & SHAFFER, D. G. 2002 Wicking flow in irregular capillaries. *Colloids Surf.* A **204** (1–3), 239–250.

SUMAN, B. & KUMAR, P. 2005 An analytical model for fluid flow and heat transfer in a micro-heat pipe of polygonal shape. *Intl J. Heat Mass Transfer* **48** (21), 4498–4509.

SZEKELY, J., NEUMANN, A. W. & CHUANG, Y. K. 1971 The rate of capillary penetration and the applicability of the Washburn equation. *J. Colloid Interface Sci.* **35**, 273–278.

WARREN, P. B. 2004 Late stage kinetics for various wicking and spreading problems. *Phys. Rev.* E **69**, 041601.

WASHBURN, E. W. 1921 The dynamics of capillary flow. *Phys. Rev.* **17**, 273–283.

WEISLOGEL, M. M. & LITCHER, S. 1998 Capillary flow in an interior corner. *J. Fluid Mech.* **373**, 349–378.

WEISLOGEL, M. M., THOMAS, E. A. & GRAF, J. C. 2009 A novel device addressing design challenges for passive fluid phase separations aboard spacecraft. *Microgravity Sci. Technol.* **21** (3), 257–268.

YOUNG, W.-B. 2004 Analysis of capillary flows in non-uniform cross-sectional capillaries. *Colloids Surf.* A **234**, 123–128.

ZHANG, J., WATSON, S. J. & WONG, H. 2007 Fluid flow and heat transfer in a dual-wet micro heat pipe. *J. Fluid Mech.* **589**, 1–32.

ZHMUD, B. V., TIBERG, F. & HALLSTENSSON, K. 2000 Dynamics of capillary rise. *J. Colloid Interface Sci.* **228**, 263–269.

https://doi.org/10.1017/jfm.2013.373 Published online by Cambridge University Press